IEEE Access
Multidisciplinary | Rapid Review | Open Access Journal

Received 9 July 2024, accepted 17 August 2024, date of publication 26 August 2024, date of current version 3 September 2024.

Digital Object Identifier 10.1109/ACCESS.2024.3450087

RESEARCH ARTICLE

Uplink Power Control Optimization for XR and eMBB Co-Existence in 5G-Advanced Networks

POURIA PAYMARD[1], (Member, IEEE), C. SANTIAGO MOREJÓN GARCÍA[2], ABOLFAZL AMIRI[2], CLAUDIO ROSA[2], BOYAN YANAKIEV[2], TROELS E. KOLDING[2], AND KLAUS I. PEDERSEN[1,2], (Senior Member, IEEE)

[1]Department of Electronic Systems, Aalborg University, 9220 Aalborg, Denmark
[2]Nokia Standards, 9220 Aalborg, Denmark

Corresponding author: Pouria Paymard (pouriap@es.aau.dk)

ABSTRACT This paper presents an analysis of fifth-generation (5G)-Advanced uplink system-level performance with the coexistence of extended reality (XR) and enhanced mobile broadband (eMBB) traffic. Dense urban (DU) and indoor hotspot (InH) deployments are studied. The study investigates the influence of uplink power control (UPC) parameters on the XR capacity and proposes strategies to manage eMBB inter-cell interference through traffic-specific UPC settings. By jointly optimizing UPC parameters for each traffic type, this research aims to minimize the eMBB throughput degradation while safeguarding the XR capacity. The findings reveal the impact of deployment scenarios on XR and eMBB capacity, and the trade-offs involved in the UPC optimization. These findings offer valuable guidance to cellular operators for optimizing network configurations to accommodate emerging XR traffic alongside existing services.

INDEX TERMS Extended reality (XR), mixed traffic, power control, 5G-advanced, system-level simulations (SLS), enhanced mobile broadband (eMBB), uplink transmission.

I. INTRODUCTION

Extended reality (XR), a collective term for augmented reality (AR), virtual reality (VR), and mixed reality (MR), is used in a large range of applications such as playing games, educational and training activities, health services, construction and design, remote industrial work, and fashion. One reference case of AR services in the uplink (UL) defined by the 3rd Generation Partnership Project (3GPP) is a 10 Mbps data rate with less than 30 ms packet delay budgets (PDBs), and 99% reliability [1]. XR traffic handling is challenging in wireless networks due to its strict quality of service (QoS) requirements on throughput, latency, and reliability. Therefore, supporting XR services demands additional research and standardization efforts.

3GPP defined in Release-17 [1] a statistical traffic model for cloud gaming, AR, and VR. It also outlined XR evaluation methods for capacity, power, coverage, and mobility, with simulations covering various deployment scenarios and frequency ranges. The findings suggested that while the current fifth-generation (5G) network supports XR, further enhancements are needed [1]. In addition, the work in [2] presents a detailed tutorial on integrating XR into the 3GPP New Radio (NR), summarizing various 3GPP service and systems aspects (SA) and radio access network (RAN) activities. It includes a system-level simulation (SLS) study evaluating the performance of different XR services over NR Release-17 and concludes with a vision for further enhancements to support XR in 3GPP NR future releases, highlighting open research problems. Release-18 [3] specified several enhancements to improve the XR performance. These included network provisions for QoS flow information, power-saving techniques like discontinuous reception (DRX) with non-integer periodicities, capacity enhancements such as multiple configured grant transmission occasions within a period (multi-PUSCH CG), and enhancements to buffer status reports (BSR). Release-19 continues the XR evolution, putting efforts into enhancing packet scheduling for UL transmissions and improving some user plane elements [4].

The associate editor coordinating the review of this manuscript and approving it for publication was Ronald Chang.

Furthermore, several studies of radio resource management (RRM) solutions, aimed to enhance XR performance in downlink (DL) over 5G-Advanced networks, have been explored in [5], [6], [7], [8], [9], [10], and [11]. Additionally, others have proposed new power-saving techniques for XR applications to improve the network power consumption in the DL direction [12], [13], [14]. Research on 5G-Advanced and sixth-generation (6G) XR enhancements is currently in progress, yet many system-level performance evaluations for XR continue to concentrate on DL cases.

The 5G UL utilizes single-carrier frequency-division multiple access (SC-FDMA) primarily due to reduced waveform peak-to-average power ratio (PAPR), reducing linearity requirements and thus power consumption in the user equipment (UE) [15]. Beyond offering lower PAPR, SC-FDMA's orthogonality effectively eliminates intra-cell interference; although sensitivity to inter-cell interference (ICI) persists. In this regard, uplink power control (UPC) is crucial, playing a pivotal role in achieving the necessary signal-to-interference-plus-noise ratio (SINR) while managing interference to neighboring cells [16]. From the system perspective, optimal UPC settings aim to minimize ICI while not compromising the user throughput, whereas, from the user standpoint, they need to be tuned to meet specific SINR requirements [17].

There are two main types of UPC: 1) closed loop power control (CLPC); and 2) open loop power control (OLPC) [18]. The OLPC sets the transmit power for the UE's basic operating point, while the CLPC may be used to further adjust the transmit power [19]. A proper setting of UPC parameters has a significant impact on the performance. However, the 3GPP specifications do not specify how to set those parameters to achieve optimal network performance. The full path-loss compensation strives to ensure that UEs in the same cell are received with the same power level at the next generation Node-B (gNB) by compensating for path loss and shadowing, disregarding the impact on neighboring cells. This method tends to increase the UL transmit power for cell-edge UEs, boosting interference to adjacent cells [17]. Given the differing interference levels from UEs at the cell edge versus those within the cell interior, fractional path-loss compensation has been introduced to mitigate ICI effectively. As path loss increases, SINR targets decrease, thus lowering the power output from cell-edge UEs and consequently reducing their interference [17]. Although effective in limiting ICI and meeting SINR requirements, the fractional approach does not guarantee fairness between UEs at different cell locations, unlike full path-loss compensation methods [20]. The fractional approach leads to a more balanced and interference-conscious network operation.

To further narrow the scope of the paper, we concentrate on the standardized OLPC scheme that serves as the primary mechanism for coordinating ICI. Here, the parameter settings for OLPC play a crucial role. Numerous studies have explored the optimization of OLPC parameters specifically for macro-only scenarios [16], [18], [19], [20], [21], [22], [23], [24], [25], and heterogeneous networks [17], [26], [27], [28], [29], [30]. Most existing studies primarily address single QoS scenarios such as enhanced mobile broadband (eMBB) services [16], [18], [19], [20], [21], [22], though some recent research also considers scenarios requiring stringent QoS such as ultra-reliable low-latency communications (URLLC) [23] as well as multi-QoS such as mixture of eMBB and URLLC [24], [25]. URLLC traffic differs significantly from XR traffic in terms of packet size and QoS requirements like latency and reliability. Given these distinctions, the application of UPC in meeting the stringent requirements of XR has not yet been thoroughly studied.

When XR and eMBB services are deployed within the same radio spectrum, the challenge of enabling their coexistence to meet mixed demands in an optimal and spectrally efficient manner is essential. To address this, the 5G standards incorporate several innovative techniques for dynamically multiplexing eMBB and XR traffic within the same spectrum. This paper focuses on the UL, aiming to jointly optimize the performance of XR and eMBB by selecting OLPC parameters that fulfill the QoS requirements of XR UEs and minimize the eMBB cell throughput degradation. To achieve this, we carry out dynamic SLS to evaluate the effects of various UPC parameters in a dynamic multi-cell 5G NR-compliant system. SLS are used due to the complexity of the system, which makes analytical solutions unattainable. This paper assesses performance in realistic deployment scenarios such as standard dense urban macro cellular (DU) and indoor hotspot (InH). These scenarios are chosen due to their distinct interference behaviors, which are crucial to understand and manage for optimal performance.

A. CONTRIBUTIONS

The primary contributions of this paper are:

- We provide insights into optimizing UL performance by identifying how UPC parameters influence the UL capacity for XR traffic in an XR-only system.
- We propose comprehensive guidelines for UPC parameter settings in mixed traffic scenarios. By jointly optimizing the UPC parameters for each traffic, we aim to minimize eMBB throughput degradation while protecting the XR capacity.
- We provide an exhaustive analysis of how eMBB UPC settings affect XR capacity performance and eMBB throughput. We also derive the eMBB throughput reduction as a function of the achieved sum rate of satisfied XR UEs. This helps in understanding the trade-offs and interactions between eMBB and XR traffic in mixed-traffic scenarios.

B. PAPER STRUCTURE

In Section II, we introduce the traffic model, 3GPP-adopted frame structure and numerology, power control, link adaptation, scheduling algorithms, key performance metrics, and network deployment models for two scenarios: DU

and InH. Section III details our simulation methodology along with confidence intervals. Section IV presents the performance results of XR-only traffic, investigating how the optimal UPC parameters enhance the XR performance. Then, Section V proposes a traffic-specific UPC algorithm and delves into the performance outcomes of mixed traffic, optimizing UPC parameters for each traffic type. Section VI recommends the best UPC combinations for different XR loads and different deployment environments. Section VII derives a new key performance indicator (KPI) to show how XR traffic affects the eMBB cell throughput degradation. Finally, in Section VIII, we draw conclusions based on the demonstrated performance benefits.

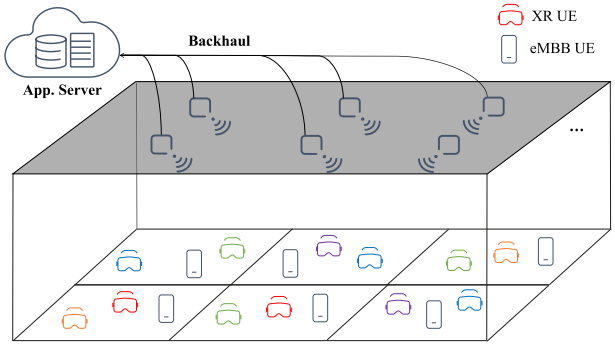

FIGURE 1. InH deployment with one eMBB and several XR UEs per cell in the DL scenario.

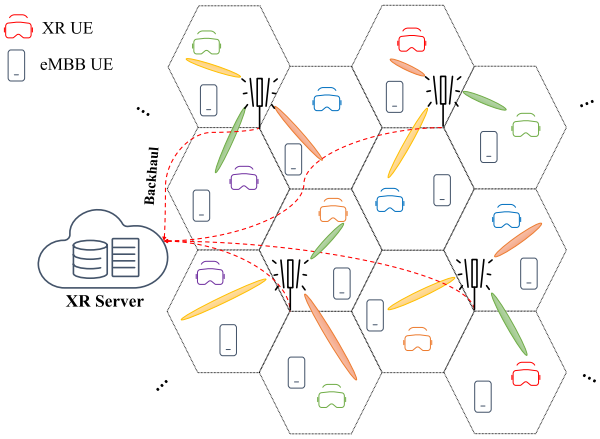

FIGURE 2. DU deployment with the existence of eMBB and XR UEs in the DL multi-cell network.

II. SETTING THE SCENE

A. NETWORK DEPLOYMENT MODEL

The InH scenario (depicted in Figure 1) consists of 12 low-power gNBs arranged in two rows within an indoor office environment. The gNB antennas are mounted on the ceiling at a height of 3 meters. The InH scenario has a 20-meter inter-site distance (ISD), and each cell covers an average area of 500 m^2. We adopt the radio propagation channel model described in [31], accounting for distance-dependent path loss, shadow fading, and fast fading, with variations depending on the line-of-sight (LOS) or non-line-of-sight (NLOS) conditions. Uniform spatial distribution of UEs within the InH scenario is assumed, where each cell has the same number of UEs. The UE antennas are positioned at a height of 1 meter. This scenario is relevant for XR gaming and remote expert assistance through virtual reality connections in indoor settings.

The second deployment, the DU scenario (shown in Figure 2), comprises high-power outdoor three-sector gNBs forming a traditional hexagonal cell grid with a 200-meter ISD. The gNB antennas are positioned above the rooftop level at a height of 25 meters. Each cell covers an approximate area of 13, 600 square meters. A 12-degree antenna down-tilt is applied to gNBs to mitigate ICI, while ensuring robust cell coverage. An even load case is assumed where UEs are uniformly distributed across cells, ensuring each cell serves the same number of UEs, e.g., 10 UEs per cell. Indoor UEs constitute 80% of the total UEs distributed uniformly across floors 1 to 6 of the buildings with equal probability. The 20% of outdoor UEs are spatially uniformly distributed at ground level with a height of 1.5 meters. The radio propagation model between gNBs and UEs considers the height of both transmitter and receiver and additional outdoor to indoor propagation loss for indoor UEs. NLOS propagation conditions are more prevalent in the DU scenario, leading to reduced ICI coupling compared to the denser InH scenarios. The DU scenario is relevant for providing reliable outdoor XR service connectivity, particularly for mobile XR UEs in diverse environments like city exploration or interactive museums. The DU and InH scenarios were central to the Release-17 (5G) and Release-18 (5G-Advanced) XR study items in 3GPP, providing complementary insights into these deployment scenarios.

B. TRAFFIC MODELS

XR applications include different traffic types e.g., video, audio, and pose in UL transmissions. For our study, we adopted video traffic for AR applications generated at the UE as described in [1]. UEs generate XR video frames, whose size is distributed according to a truncated Gaussian distribution $\Gamma_{vf} \sim TN(\mu_\Gamma, \sigma_\Gamma, a_\Gamma, b_\Gamma)$, where the average value and the standard deviation are expressed by μ_Γ and σ_Γ, respectively. In alignment with [1], the assumed data rate for XR video is 10 Mbps at 60fps, translating into a mean value of 20838 bytes/frame. The truncation limits are minimum value $a_\Gamma = 0.5\mu_\Gamma$ to a maximum of $b_\Gamma = 1.5\mu_\Gamma$, corresponding to 10419 bytes/frame and 31257 bytes/frame, respectively. At the UE, the XR video frames arrive without jitter and with an inter-frame arrival of 16.67 ms.

The traffic model assumed for eMBB is the infinite buffer, also known as the *full-buffer* model, where each UE has a full buffer of data awaiting transmission to the serving gNB. Having UEs with full-buffer traffic in all cells results in a constant full-load regime in the entire network. Despite its simplicity, this model is valuable in analyzing extensive eMBB data uploads. Furthermore, it adds to understanding

how the XR traffic influences the data rates experienced by eMBB UEs. This identical eMBB full-buffer traffic model has been employed in previous studies examining the collective performance of XR and eMBB DL performance in InH and DU scenarios [32], [33].

C. FRAME STRUCTURE AND NUMEROLOGY

We use SC-FDMA as the 3GPP-adopted UL multiple access. Fixed time division duplexing (TDD) with DDDSU slots, where D, S, and U denote DL, special, and UL slots, respectively, is assumed. Each slot comprises 14 orthogonal frequency-division multiplexing (OFDM) symbols, based on a subcarrier spacing (SCS) of 30 kHz, resulting in a slot duration of 0.5 ms. Within the S slot, there are ten DL symbols, accompanied by two guard symbols and two UL symbols. Nevertheless, UL data transmissions exclusively occur within the U slots. Thus, there is only one opportunity for UL data transmissions every 2.5 ms. We account for the overhead of the physical uplink control channel (PUCCH), demodulation reference signal (DMRS), and other control signals by assuming that the first OFDM symbol in the U slots, as well as the two UL symbols in the S slots, are not used for data transmission. Given a carrier bandwidth of 100 MHz and an SCS of 30 kHz, the spectrum will be divided into 272 physical resource blocks (PRBs), each PRB comprising 12 subcarriers.

D. LINK ADAPTATION AND PACKET SCHEDULING

The link adaptation (LA) algorithm allows a gNB to dynamically adjust the modulation schemes and code rates based on its assessment of channel quality in the form of the measured SINR. It determines the optimal modulation and coding scheme (MCS) for a radio link, subject to satisfying a target block error rate (BLER) of e.g., 10%. The selected MCS is sent to the UE in a scheduling grant, along with other scheduling details. Upon successful reception of the UL scheduling grant, the UE generates an UL transport block (TB) according to the grant and transmits the TB over the UL slot. To estimate the SINR, the gNB performs signal strength measurements transmitted by the UEs, along with interference measurements. These measurements are utilized to determine the SINR and subsequently select the most appropriate MCS. The described LA algorithm is inherently susceptible to scheduling delays, variability in interference, etc. These factors may lead to deviations in the experienced BLER from the predefined target during initial transmission. Consequently, an outer loop link adaptation (OLLA) algorithm is employed adjusting the estimated SINR by an offset before MCS selection. The LA algorithm employed in this paper is consistent with the one proposed in [2].

We assume an adaptive transmission bandwidth (ATB) scheduling algorithm as described in [34]. Under ATB, based on a frequency-selective metric such as proportional fair (PF) metric, the gNB schedules PRBs to UEs within a transmission

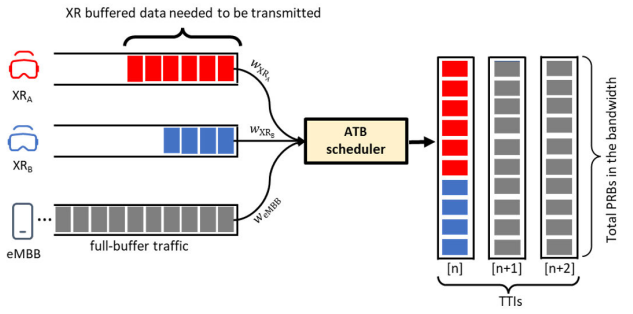

FIGURE 3. Example of ATB scheduling for two different UE groups (eMBB and XR).

time interval (TTI). The ATB scheduler prioritizes XR transmissions over eMBB transmissions. Hybrid automatic repeat request (HARQ) retransmissions are prioritized over new transmissions for each traffic class. Since we assumed SC-FDMA, the allocation of PRBs must be contiguous ensuring that a UE is assigned neighboring PRBs without any gaps in the allocation. Specifically, a UE's PRB allocation stops if either the UE has no further data to transmit, or it has reached its maximum transmission power, or there are no additional available PRBs. An example of ATB scheduling for XR and eMBB traffic is shown in Figure 3.

E. UPLINK POWER CONTROL

UPC consists in setting the UE's transmit power, to fulfill network coverage and capacity demands. Increasing the UE transmit power results in better SINR, while decreasing it reduces the generated co-channel interference to neighboring cells. Therefore, improper UPC settings may lead to poor performance, particularly in scenarios with many cell-edge UEs located far from the gNB. This can result in high interference, call drops, and reduced throughput. Hence, optimizing the UPC setting is essential for service providers to meet the QoS requirements for different UE classes, as well as to ensure the required UE power consumption. The UE transmit power is expressed, in dBm, as follows [23]:

$$P_{tx} = \min\left\{P_{CMAX}, 10\log_{10}(B) + P_0 + \alpha \times PL + \Delta\right\} \quad (1)$$

where P_{CMAX} is the UE's-configured maximum output power in dBm, B is the number of allocated PRBs to the UE, and PL is the estimated path loss between the serving gNB and the UE, in dB. P_0 is a pre-configured received target power level per physical resource block, assuming full path-loss compensation, in dBm. $\alpha \in [0, 1]$ is the fractional power control compensation factor. $\alpha = 0$ corresponds to no path-loss compensation, i.e., all UEs transmit at the same power spectral density, while $\alpha = 1$ corresponds to full path-loss compensation, with the intent to achieve equal received power spectral density for all UEs. Δ is a closed-loop power control component that allows the gNB to adjust the transmit power of each UE, in dB. The agreed UPC scheme relies on an OLPC algorithm to handle slow channel variations, therefore, $\Delta = 0$.

F. KEY PERFORMANCE INDICATORS

Different KPIs are employed to evaluate the performance of both traffic types, XR and eMBB. Following, the 3GPP evaluation methodology [1], [3], we adopt the primary KPIs for XR studies. An XR UE is said to be satisfied if 99% of the packets are correctly received by the serving gNB within the required PDB, which is 30 ms for AR UL video frames. First and foremost, the 3GPP-defined XR satisfaction ratio is calculated by dividing the number of satisfied UEs by the total number of XR UEs in the network. Also, XR capacity KPI is defined as the maximum supported number of XR UEs per cell, maintaining an XR satisfaction ratio of at least 90%. Moreover, we consider the average cell throughput as the main KPI for eMBB UEs. It is collected across all eMBB UE throughput samples within the cell, and then, it is averaged over the cells in the network. We also analyze the standard radio performance KPIs such as the average percentage of utilized PRBs in the network, experienced post-detection SINR after interference rejection combining, UL packet delay, and UE's transmit power.

III. EVALUATION METHODOLOGY

We use dynamic SLS to assess the performance of the system model presented in the previous section. The SLS includes 3GPP-endorsed models for performance-determining effects, in line with the recently published tutorial on SLS in [35], with most of the RAN functions implemented. Different network deployments of gNBs and radio propagation are modeled. The utilization of the UE's transmit power and OLPC mechanism are accurately modeled.

The cell selection is determined by the reference signal received power (RSRP) measurements, ensuring each user is served by the cell with the highest RSRP. The UEs' traffic follows a specified traffic model, and it is buffered in the UE until successfully transmitted. All transmissions are with multiple-input and multiple-output (MIMO) using rank 1 and spatial diversity mode with the open loop Alamouti scheme. In this study, the gNB assumes ideal and instantaneous information about the UE's buffer occupancy, meaning there is no effect of scheduling requests or buffer status reports modeled. The gNB manages scheduling grants to its UEs' UL transmissions. The ATB scheduling policy determines the timing of data transmission to UEs, and the selection of PRBs based on the proportional fairness metric, while LA selects the highest MCS index while ensuring a block error probability of 10%.

For each UE transmission to its serving cell, the received signal at the gNB is calculated within the SLS, factoring in the effects of the transmit antenna array, radio propagation, and UE antennas. Additionally, the SLS computes the aggregated interference from other UEs in the system on the PRBs of the desired signal. Based on this, the received SINR is calculated per symbol and sub-carrier of the radio resources of the transmitted signal from the UE. These SINR values are used to compute the effective SINR of the transmission, using the mean mutual information per coded bit (MMIB) [36] to determine if the transmission is correctly decoded. A lookup table derived from link-level simulations is used for this last step. For unsuccessful transmissions, a negative acknowledgment is sent back to the UE. Additional details regarding the SINR calculations for minimum mean square error-interference rejection combining (MMSE-IRC) receivers, can be found in [37]. A summary of important SLS parameters is outlined in Table 1.

TABLE 1. Summary of system-level evaluation parameters.

Parameter	Setting	
Deployment	InH	DU
World Area	120 m × 50m	528 m × 460 m
Layout	12 cells	21 cells
Inter-site Distance	20 m	200 m
gNB height	3 m	25 m
gNB down tilt	90°	12°
Indoor UE probability	1	0.8
Number of building floors	1	6
UE distribution per floor	-	uniform(1, 6)
Simulation time	10 sec per run	
Simulation runs	10 runs	
TDD Frame structure	DDDSU	
TTI length	14 OFDM symbols	
PUCCH/DMRS overhead	1 OFDM symbol	
Carrier frequency	4 GHz	
Bandwidth	100 MHz	
SCS	30 kHz	
UE transmit power	23 dBm	
UE height	1.5 m	
Number of UE antennas	2 Tx antennas	
gNB receiver	MMSE-IRC	
gNB antenna	1 panel with 32 elements (4×4 and 2 polarization)	
number of eMBB UEs/cell	10	
XR frame rate	60 fps	
XR source data rate	10 Mbps	
XR PDB	30 ms	
Scheduler	ATB	
XR priority	High	
eMBB priority	Low	
HARQ combining method	Chase combining	
Cell Selection	RSRP Slow Fading	
BLER Target	10%	
Modulation	QPSK to 64QAM	

To ensure a reliable performance evaluation, each XR UE transmits at least 600 XR video frames. This allows us to confidently state that 99% of packets meet the PDB criteria with a 95% confidence level and an error margin of ±1%. Our simulations track N XR UEs per cell across C cells, totaling statistics for $C \times N$ UEs. We execute M simulation drops where UEs are randomly relocated in order to have sufficient statistics for different UE positions. Our final statistics include $C \times N \times M$ XR UEs. In the case of InH, we use $N = 8$, $C = 12$, and $M = 10$, generating statistics for 960 XR UEs. This dataset enables us to assert, with 95% confidence, that 90% of XR UEs satisfy the XR capacity definition metric, within an error margin of ±2%. This approach also effectively monitors throughput samples per TTI and accurately evaluates the average cell throughput for eMBB UEs.

IV. PERFORMANCE RESULTS: UPC PARAMETER OPTIMIZATION FOR XR-ONLY NETWORKS

As the satisfaction of cell-edge XR UEs is as important as that of cell-center UEs, we select values of α to be close to 1 (e.g., 0.8 and 1) to ensure XR service quality for both cell-center and cell-edge UEs. However, this must be combined with lower P_0 values to prevent excessive network interference.

Figure 4 illustrates the satisfaction ratio as a function of P_0 for DU (in Figure 4(a)) and InH (in Figure 4(b)) deployments, featuring full ($\alpha = 1$) and fractional ($\alpha = 0.8$) path-loss compensation. Different XR loads (i.e., the number of XR UEs per cell) are considered. The results show that optimal UPC settings vary with the number of XR UEs and deployment scenarios. For instance, optimal P_0 values differ between loads of 2 and 4 UEs per cell in DU, consistent with previous findings on load adaptive power control in long-term evolution (LTE) [22]. This implies that the setting of P_0 and α should in principle be set as a function of the number of XR UEs per cell to achieve the best performance. However, as observed from the results, there are only modest variations of the performance for different loads, so using one OLPC parameter setting for different XR would lead to near-optimal performance in practice.

In Figure 4(a), with fractional path-loss compensation and $P_0 = -93$ dBm is the only value that can support an XR capacity of 4 UEs per cell (i.e. with a satisfaction ratio greater than 90%). With full path-loss compensation for DU, the maximum capacity is achieved for $P_0 = -115$ dBm, supporting up to 4 satisfied XR UEs per cell. Furthermore, even in the low load scenario with 1 or 2 UEs per cell, approximately $2-5\%$ of XR UEs are unsatisfied in DU due to UE transmit power limits affecting their PRB utilization.

Figure 4(b) shows a wider range of best P_0 values for both full and fractional path-loss compensation. Here it is observed that any P_0 value between -85 dBm to -75 dBm provides the maximum XR capacity for full path-loss compensation. However, taking other performance metrics like XR UE's transmit power and PRB allocation into account, the optimal setting in InH with full path-loss compensation occurs at $P_0 = -97$ dBm, while it occurs at $P_0 = -85$ with fractional path-loss compensation, supporting up to 8 satisfied UEs per cell. This conclusion is derived from the UPC settings that support up to 8 satisfied UEs per cell, showing the lowest observed UE transmit power and PRB utilization.

Figure 5 presents the empirical cumulative distribution function (CDF) of the Network's PRB utilization per TTI for cases with 4 and 8 XR UEs per cell in DU and InH (maximum supported capacity), respectively. The CDF is built on the collection of the average PRB utilization across all cells in the network for each TTI. The UPC setting with $\alpha = 0.8$ and $P_0 = -93$ dBm results in 27% lower resource utilization at the 50-percentile compared to full path-loss compensation. In the InH scenario, there is no difference between the fractional and full path-loss compensation. The average PRB utilization is approximately 55% in DU with fractional path-loss compensation for the maximum number of supported XR UEs per cell. However, the average PRB utilization rises to about 90% in InH.

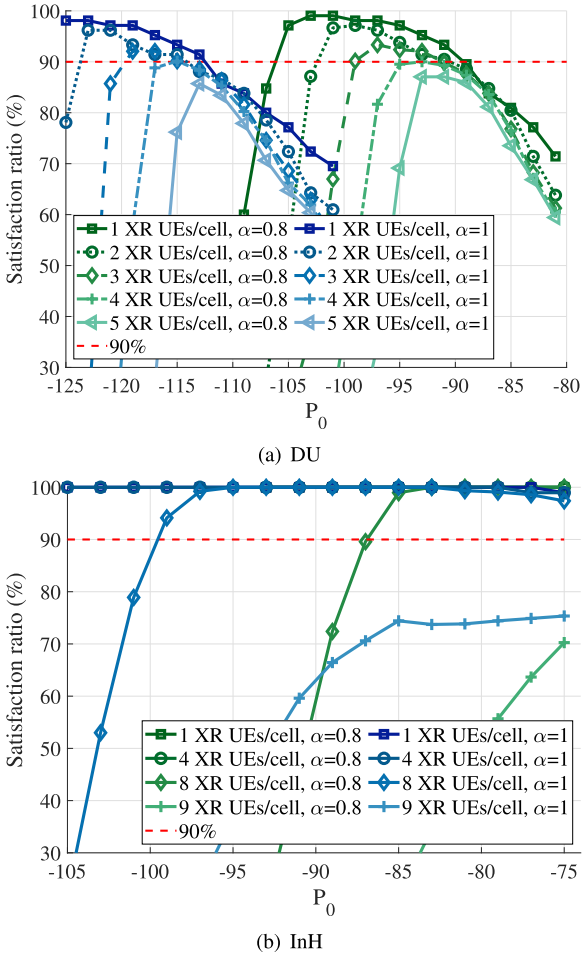

FIGURE 4. UE satisfaction ratio versus P_0 for different numbers of connected UEs per cell in different deployments.

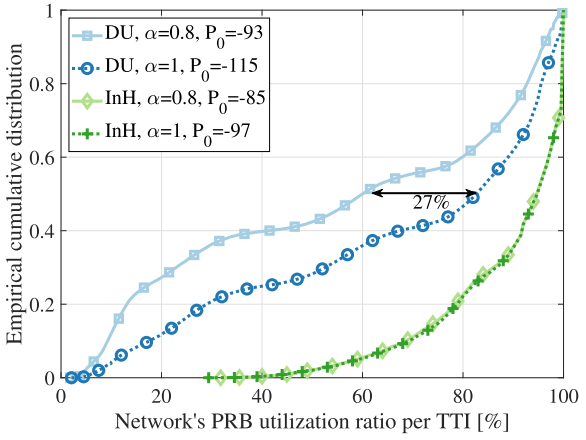

FIGURE 5. The empirical CDF of the Network's PRB utilization ratio per TTI for different deployment scenarios.

The empirical CDF of the UE's UL transmit power is depicted in Figure 6 for both DU and InH deployments under different UPC settings. There is a slight transmit

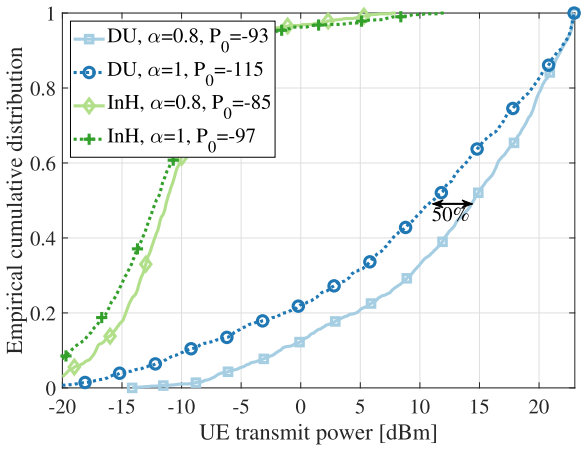

FIGURE 6. The empirical CDF of UL transmit power for XR UEs.

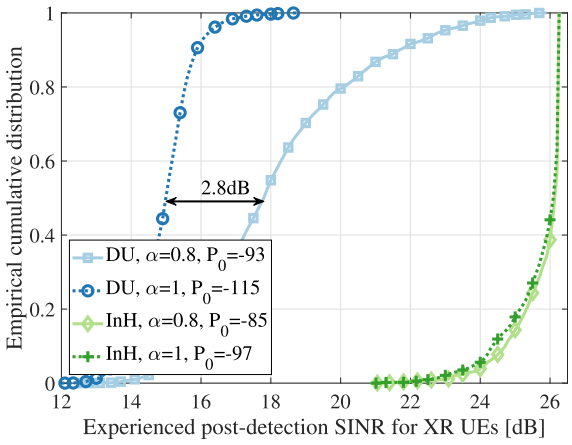

FIGURE 7. The empirical CDF of experienced SINR for XR UEs.

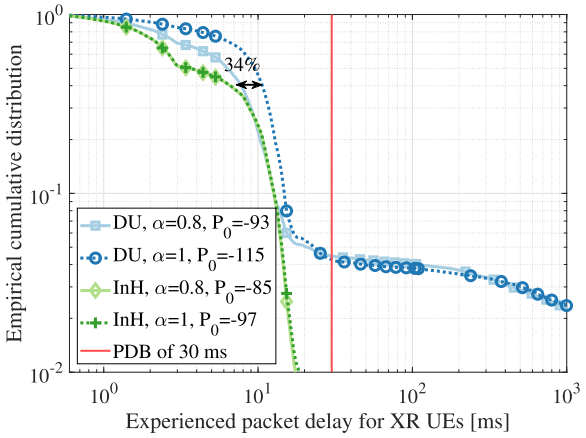

FIGURE 8. The empirical CDF of experienced UL delay for XR UEs.

power reduction with full path-loss compensation in the InH scenario compared to the fractional path-loss compensation. However, there is a significant transmit power reduction with full path-loss compensation compared to fractional path-loss compensation in the DU scenario, showing that a higher P_0 typically results in a higher received signal power level. For example, the used transmit power is 3 dB lower with full path-loss compensation than with fractional path-loss compensation in DU at the 50-percentile of the CDF. This corresponds to approximately 50% of the transmit power in Watts, indicating significant UE power consumption savings and providing greater power headroom. Furthermore, the significantly lower transmit power observed in InH deployments compared to DU is a direct consequence of the larger cell size in DU environments. The larger cell size in DU environments necessitates higher transmit power.

Concluding from Figures 5 and 6, the DU scenario is UE transmit power-limited, as edge UEs operating close to their maximum transmit power cannot transmit with large bandwidth. This can be observed in Figures 5 and 6, where the DU scenario shows high UE transmit power and relatively low resource utilization. In contrast, the InH scenario is resource-limited, as indicated by the high resource utilization achieved with relatively low UE transmit power.

Figure 7 illustrates the empirical CDF of post-detection SINR. The results highlight a notable SINR improvement for the XR UEs in the DU scenario with fractional path-loss compensation compared to full path-loss compensation, with a median SINR gain of approximately 2.8 dB. This SINR gain can be attributed to the higher transmit power associated with fractional path-loss compensation, which increases the received signal power spectral density, potentially improving SINR even if the interference level remains the same or increases less than the transmit power. Conversely, the SINR improvement in the InH scenario is minimal, indicating that SINR levels are already sufficiently high due to the closer proximity of UEs to gNBs and smaller cell sizes. When comparing the InH and DU scenarios, it becomes clear that SINR levels are consistently higher in the InH scenario than in DU, reflecting the different interference and propagation conditions.

Figure 8 illustrates the impact of UPC settings on the UL packet delay statistics. The empirical CDF of UL latency reflects the latency from the moment an XR payload reaches the packet data convergence protocol (PDCP) layer of the UE until it is successfully received at the gNB's PDCP layer. This latency encompasses queuing delays at the UE and gNB, transmission time, and processing times at both end-points, including the potential effects of HARQ retransmissions. The figure shows a 34% reduction at the 50-percentile of delay CDF with fractional path-loss compensation in the DU scenario compared to full path-loss compensation. This improvement is due to higher UE SINR levels, which causes the selection of higher MCS indexes, leading to increased throughput and reduced transmission times. Despite this delay improvement in DU, we still observe that it remains insufficient to meet the minimum XR requirements (delivery of 99% of UL packets within the PDB of 30 ms). This limitation suggests that the available power and PRBs are not sufficient to support an additional UE under the current cell size. So, if the inter-site distance were reduced, it might potentially allow for an extra satisfied UE in DU.

Furthermore, as indicated in Figure 7, the SINR improvement in the InH scenario is minimal, resulting in no visible difference in delay between the two UPC settings for InH.

Based on the analyses in this section, the optimal UPC settings for supporting the highest number of XR UEs per cell are $\{P_0^{\text{XR}} = -93$ dBm, $\alpha^{\text{XR}} = 0.8\}$ and $\{P_0^{\text{XR}} = -115$ dBm, $\alpha^{\text{XR}} = 1\}$ for DU. These configurations ensure high-quality XR service for both cell-center and cell-edge UEs. However, full path-loss compensation requires more PRBs for XR UEs, leaving fewer PRBs for other services like eMBB in the co-existence scenario. Therefore, we recommend using $\{P_0^{\text{XR}} = -93$ dBm, $\alpha^{\text{XR}} = 0.8\}$ for DU in the subsequent sections. Furthermore, SINR, delay, and average PRB utilization are similar between full and fractional path-loss compensation settings (i.e., $\{P_0^{\text{XR}} = -85$ dBm, α^{XR}=0.8$\}$ and $\{P_0^{\text{XR}} = -97$ dBm, $\alpha^{\text{XR}} = 1\}$), indicating that either UPC setting can be used for InH without significant differences.

V. PERFORMANCE RESULTS: UPC PARAMETER OPTIMIZATION FOR MIXED-TRAFFIC NETWORKS

In the DU scenario with full XR capacity, the network's average PRB utilization per TTI is approximately 50%, as shown in Figure 5. Adding eMBB UEs with the same UPC settings can result in increased PRB utilization leading to increased interference, which may impact XR performance. This observation led us to hypothesize that traffic-specific UPC settings could be beneficial in managing the trade-off between XR and eMBB performance. To assess this hypothesis, we first examined the impact of adding eMBB UEs with the same UPC settings as XR UEs. The results showed increased interference, negatively affecting XR performance. Given the distinct QoS requirements and characteristics of eMBB and XR services, it became clear that a one-size-fits-all approach to UPC settings is suboptimal. eMBB services benefit from higher throughput, while XR services require a guaranteed bit rate, stringent latency, and high reliability. This makes XR UEs more sensitive to ICI and UPC needs. Both eMBB and XR UEs can be located at the cell center or cell edge, but they still require distinct UPC settings due to their different QoS requirements and characteristics.

To reduce inter-cell interference generated by eMBB UEs, it is beneficial to control their transmit power, which helps protect XR UEs. By setting different UPC parameters for each traffic type, it is possible to manage this trade-off effectively. Specifically, adjusting the UPC settings for eMBB UEs can help minimizing their interference on XR UEs, thereby maintaining the QoS for XR while also optimizing eMBB performance.

The 5G specifications allow for different OLPC settings per UE. Our proposal leverages this capability by applying service-specific UPC settings to optimize performance for both eMBB and XR traffic. eMBB UEs are configured with P_0^{eMBB} and α^{eMBB}, while XR UEs are configured with P_0^{XR} and α^{XR}. For simplicity, we assume all UEs in a cell use the same parameters for each service. These parameters must be carefully selected to meet service requirements. For instance, setting P_0^{eMBB} significantly higher than P_0^{XR} with $\alpha^{\text{XR}} = \alpha^{\text{eMBB}}$ can increase eMBB interference over XR, compromising XR capacity, whereas P_0^{eMBB} much lower than P_0^{XR} can deteriorate eMBB throughput. As seen in Section IV, the best UPC setting for the highest number of supported XR UEs per cell occurs in $\{P_0^{\text{XR}} = -93$ dBm, $\alpha^{\text{XR}} = 0.8\}$ for DU. Although there were no remarkable differences between full and fractional path loss compensation, we have selected $\{P_0^{\text{XR}} = -85$ dBm, $\alpha^{\text{XR}} = 0.8\}$ for InH. These settings ensure XR service quality for both cell-center and cell-edge UEs. To optimize eMBB throughput without compromising the optimal performance of XR services, we choose the values of $\alpha^{\text{eMBB}} = \{0.6, 0.8, 1\}$ and sweep over P_0^{eMBB}. This approach allows us to balance the performance between cell-center and cell-edge UEs, ensuring a compromise that maintains high-priority XR capacity while evaluating eMBB performance using the primary KPI of eMBB cell throughput.

A. THE IMPACT OF TRAFFIC-SPECIFIC UPC ON THE XR PERFORMANCE

Figure 9 illustrates the XR satisfaction ratio versus P_0^{eMBB} for DU (in Figure 9(a)) and InH (in Figure 9(b)) deployments, featuring three different α^{eMBB} values. The maximum supported XR load for an XR-only scenario (i.e., 4 UEs per cell for DU, and 8 UEs per cell for InH) is assumed. The results demonstrate that optimal UPC settings vary with deployment scenarios. The optimality criteria are defined as maintaining an XR satisfaction ratio above 90%. For example, in Figure 9(a), given $\alpha^{\text{eMBB}} = 0.8$, the XR satisfaction ratio remains above 90% as long as -117 dBm $\leq P_0^{\text{eMBB}} \leq -95$ dBm. However, the pair $\{P_0^{\text{eMBB}} = -93$ dBm, $\alpha^{\text{eMBB}} = 0.8\}$, which corresponds to the same UPC setting as XR-only (i.e., $\alpha^{\text{XR}} = \alpha^{\text{eMBB}}$, $P_0^{\text{XR}} = P_0^{\text{eMBB}}$), does not reach the 90% satisfaction ratio target. This means that the XR capacity reduces to 3 UEs per cell in DU and implies a 25% degradation in XR capacity compared to the XR-only scenario shown in Figure 9(a). This observation emphasizes the need for per-traffic UPC optimization in a DU scenario. However, Figure 9(b) shows a wider range of UPC settings for the InH scenario, where any P_0^{eMBB} value between -104 dBm and -52 dBm (simulated range) for $\alpha^{\text{eMBB}} \in \{0.6, 0.8, 1\}$ provides the maximum XR capacity. This is because, with the maximum number of XR UEs, there are very few PRBs available for eMBB traffic, making the eMBB UPC settings less impactful as eMBB traffic scheduling is minimal. However, if we consider a scenario with fewer XR UEs, such as 4 XR UEs in InH, there would be more PRBs available for eMBB traffic. In such a case, the settings of eMBB UPC parameters would have a notable impact on the network performance.

B. THE IMPACT OF TRAFFIC-SPECIFIC UPC ON THE eMBB PERFORMANCE

In this subsection, we pick the best UPC combinations from Figure 9 that support the highest XR capacity. For

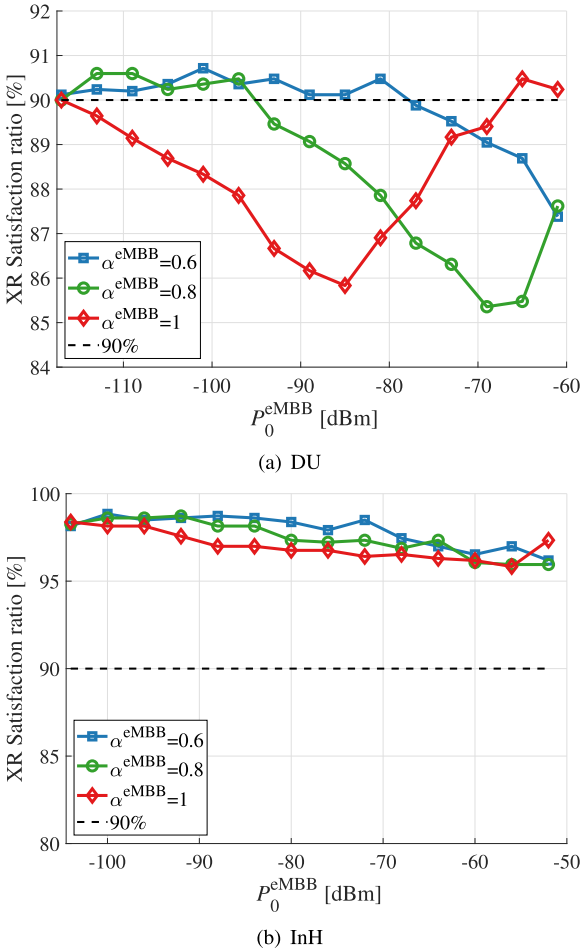

FIGURE 9. XR satisfaction ratio versus P_0 for different α values in different deployments.

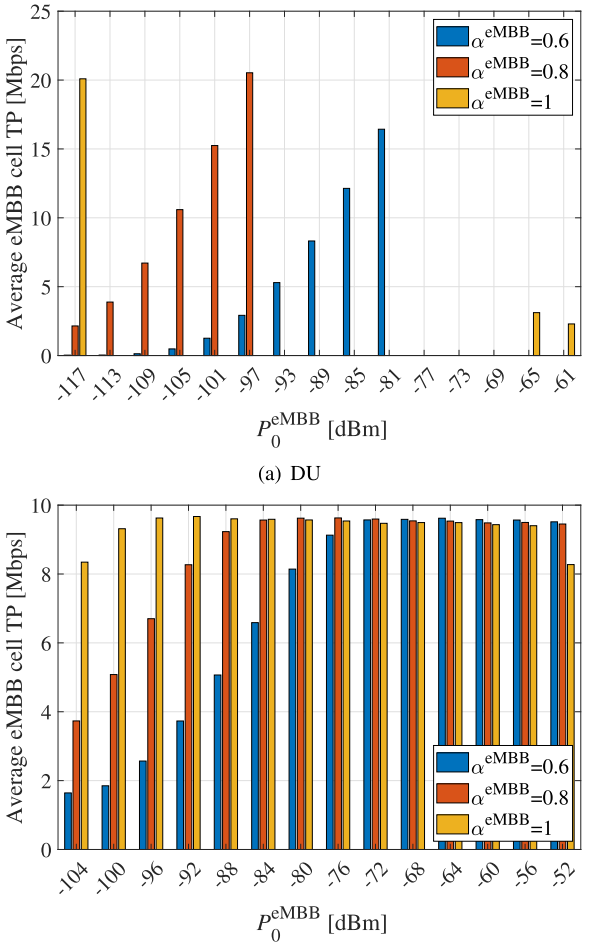

FIGURE 10. Average eMBB cell throughput versus different values of P_0 for various α values that maintain the XR satisfaction ratio above 90% at the maximum number of supported XR UEs per cell across different deployments.

the DU scenario, this corresponds to 4 XR UEs per cell, and for the InH scenario, 8 XR UEs per cell. Figure 10 shows the average eMBB cell throughput for the maximum supported XR UEs per cell as a function of P_0^{eMBB} and α^{eMBB}. As seen, the UPC combinations significantly affect the eMBB throughput in both DU and InH. In Figure 10(a), we observe the three pairs of $\{\alpha^{eMBB} = 1, P_0^{eMBB} = -117$ dBm$\}$, $\{\alpha^{eMBB} = 0.8, P_0^{eMBB} = -97$ dBm$\}$, and $\{\alpha^{eMBB} = 0.6, P_0^{eMBB} = -81$ dBm$\}$ outperform the other UPC settings, not only fulfilling the XR UEs satisfaction ratio but also providing the highest eMBB average cell throughputs. The best combination is $P_0^{eMBB} = -97$ dBm and $\alpha^{eMBB} = 0.8$ as it provides slightly better eMBB throughput and XR satisfaction ratio. Figure 10(b) shows a wider range of UPC settings that provide the highest eMBB cell throughput. For example, there is a negligible difference in the eMBB throughput in the range of $-96 \leq P_0^{eMBB} \leq -56$ with $\alpha^{eMBB} = 1$ for the InH scenario. This is because the channel conditions are excellent in InH no matter which of the best UPC settings are adopted.

It is important to note that selecting the best UPC parameter for eMBB based solely on average cell throughput can be misleading. High average cell throughput may come at the expense of low cell-edge UE eMBB throughput, which can negatively impact overall network performance. Thus, we also include cell-edge eMBB throughput to ensure balanced and optimal performance across the network. Figure 11 illustrates cell-edge eMBB throughput for the best UPC combinations that support the highest XR capacity. The general trend is similar to Figure 10. In Figure 11(a), UPC combinations of $\{\alpha^{eMBB} = 1, P_0^{eMBB} = -117$ dBm$\}$, $\{\alpha^{eMBB} = 0.8, P_0^{eMBB} = -97$ dBm$\}$, and $\{\alpha^{eMBB} = 0.6, P_0^{eMBB} = -81$ dBm$\}$ outperform the other UPC settings, not only fulfilling the XR UEs satisfaction ratio but also providing the highest eMBB average cell throughputs and eMBB cell-edge throughput. Figure 11(b) shows a wider range of UPC pairs that provide the highest eMBB cell-edge throughput. For example, there is a negligible difference in the eMBB throughput in the range of $-72 \leq P_0^{eMBB} \leq -52$ with $\alpha^{eMBB} = 0.6$ for the InH scenario. This is because the channel conditions are excellent (no difference between cell-edge and cell-center UEs) in InH no matter which of the best UPC settings are adopted.

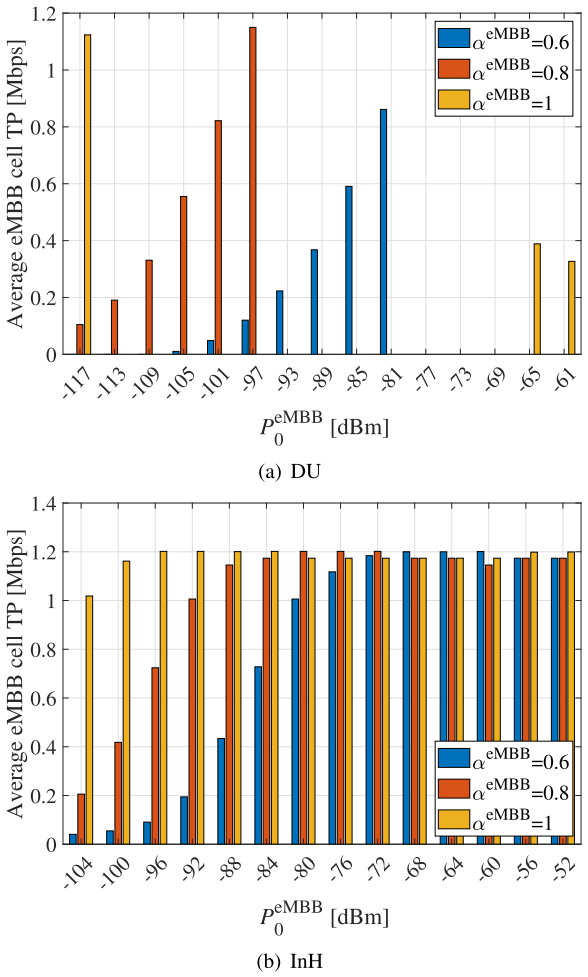

FIGURE 11. The eMBB cell-edge throughput versus different values of P_0 for various α values that maintain the XR satisfaction ratio above 90% at the maximum number of supported XR UEs per cell across different deployments.

VI. PRACTICAL GUIDELINES ON UPC SETTINGS

Drawing from Section IV and Section V, we have obtained different UPC settings that provide the best performance for the network and UE requirements. The proper configurations are outlined in Table 2 for various numbers of XR UEs per cell. The table shows the UPC variability in different deployment scenarios and concludes that the proper UPC setting varies with cell load. The InH results demonstrate a broader range of optimal P_0^{XR} values for both full and fractional path-loss compensation. However, when considering other performance metrics, such as XR UE's transmit power and PRB allocation, the optimal setting in InH with full path-loss compensation is $P_0^{\text{XR}} = -97$ dBm, and with fractional path-loss compensation, it is $P_0^{\text{XR}} = -85$ dBm. These settings support up to 8 satisfied UEs per cell.

Furthermore, Table 3 summarizes the best UPC combinations for eMBB UEs in different deployments. Combinations are obtained from Figure 10. The table suggests using different UPC configurations for eMBB and XR in the DU scenario because the XR satisfaction ratio falls below the

TABLE 2. Practical guidelines on UPC settings in both DU and InH for different numbers of XR UEs per cell.

DU		InH	
# $\frac{\text{XR UE}}{\text{Cell}}$	UPC setting $\{\alpha^{\text{XR}}, P_0^{\text{XR}}\}$	# $\frac{\text{XR UE}}{\text{Cell}}$	UPC setting $\{\alpha^{\text{XR}}, P_0^{\text{XR}}\}$
1	$\{0.8, -101$ dBm$\}$	1	$\{0.8, -93 \leq P_0^{\text{XR}} \leq$ -75$\}$ $\{1, -105 \leq P_0^{\text{XR}} \leq$ -77$\}$
2	$\{0.8, -98$ dBm$\}$	4	$\{0.8, -83 \leq P_0^{\text{XR}} \leq$ -75$\}$ $\{1, -91 \leq P_0^{\text{XR}} \leq$ -79$\}$
3	$\{0.8, -95$ dBm$\}$	8	$\{0.8, -85$ dBm$\}$ {1, -97 dBm}
4	$\{0.8, -93$ dBm$\}$	-	-

TABLE 3. Practical guidelines on the best UPC settings for eMBB UEs in both DU and InH to protect XR capacity.

DU		
UPC combination $\{\alpha^{\text{eMBB}}, P_0^{\text{eMBB}}\}$	XR Satisfaction ratio (%)	Avg. eMBB Cell Throughput (Mbps)
C_1: $\{-117, 1\}$	90	20
C_2: $\{-97, 0.8\}$	90.5	20.5
C_3: $\{-81, 0.6\}$	90.5	16.5
InH		
C_1: $\{-96, 1\}$	98	9.6
C_2: $\{-84, 0.8\}$	98	9.6
C_3: $\{-72, 0.6\}$	98	9.6

90% target when eMBB UEs use the same UPC settings as XR UEs. Therefore, a service-specific UPC configuration is necessary to optimize performance for both traffic types. Additionally, the impact of XR UEs on eMBB is minimized in the DU scenario with UPC configuration C_2, which we recommend for this scenario. In the InH scenario, all three UPC sets presented in Table 3 yield similar performance.

VII. THE eMBB CELL THROUGHPUT REDUCTION FACTOR

We define the eMBB cell throughput reduction factor as the ratio of the average eMBB cell TP degradation to the achieved sum rate of satisfied XR UEs, expressed as:

$$\zeta(P_0^{\text{eMBB}}, \alpha^{\text{eMBB}}) = \frac{R_{\text{eMBB-Only}} - R_{\text{eMBB-Mixed}}}{R_{\text{XR}} \times C_{\text{XR}}}, \quad (2)$$

where $R_{\text{eMBB-Only}}$ and $R_{\text{eMBB-Mixed}}$ are the eMBB cell throughput for eMBB-only and mixed traffic scenarios as a function of the UPC setting, respectively. R_{XR} is the XR source data rate (i.e., 10 Mbps). C_{XR} represents XR capacity (maximum supported XR UEs per cell) as a function of the UPC setting. After a series of simulations, the maximum value of $R_{\text{eMBB-Only}}$ is determined to be about 90.5 (91.2) Mbps in the DU (InH) scenario, respectively.

Table 4 summarizes ζ results for different UPC combinations in both InH and DU scenarios. For example, $\zeta = 1$ means the decrease in eMBB average cell throughput is equal to the increase in added XR throughput. The key

TABLE 4. The eMBB cell throughput reduction factor in InH and DU scenarios for different eMBB UPC settings that protect XR capacity.

	C_1	C_2	C_3
InH	1.02	1.02	1.02
DU	1.76	1.75	1.85

takeaway from Table 4 is that the impact of XR UEs on eMBB throughput varies depending on the specific deployment scenario and chosen UPC settings.

The most significant impact on eMBB throughput occurs in the C_3 DU scenario. In this case, the network prioritizes managing ICI by choosing $P_0^{\text{eMBB}} = 0.6$ even if it comes at the cost of sacrificing some throughput for devices located at the edge of the cell (cell-edge UE throughput). This trade-off is reflected in the value of $\zeta = 1.85$ in C_3. This means that adding 4 XR UEs reduces the overall eMBB throughput by $1.85 \times 4 \times 10$ Mbps in this specific scenario. Additionally, the impact of XR UEs is minimized in the DU scenario with C_2. This suggests that the UPC configuration in this scenario strikes a better balance between managing interference and maintaining eMBB throughput.

Interestingly, the impact of XR UEs on eMBB throughput remains relatively consistent across all UPC settings in InH deployments. This is because InH environments typically have high SINR levels. Additionally, the limited availability of PRBs is the primary bottleneck in InH deployments, not interference. As a result, the value of $\zeta \approx 1$ in the table indicates that adding 8 XR UEs in an InH environment might only reduce eMBB throughput by 8×10 Mbps, highlighting a less significant impact compared to the DU scenario in C_3.

Understanding these findings is crucial for optimizing mobile network configurations to accommodate the growing demand for XR applications. By carefully selecting UPC settings in different deployments, network operators can ensure a balance between supporting XR experiences and maintaining optimal eMBB performance.

VIII. CONCLUSION

In this paper, we have shown the importance of optimizing the UPC settings for different deployment scenarios to maximize XR capacity while obtaining the best possible best-effort eMBB throughput in the system. For the InH and DU scenarios, optimizing UPC parameters allows supporting up to 8 or 4 satisfied XR UEs per cell, respectively, each with 10 Mbps guaranteed average throughput and a 30 ms PDB at 99% reliability.

- For the DU scenario, the optimal UPC setting is sensitive to the number of supported XR UEs, suggesting that load-adaptive UPC settings should be used to achieve the best possible performance. UE transmit power limitations often prevent scheduling the XR UE(s) on all available PRBs, resulting in approximately $2-5\%$ of the XR UEs not being fully satisfied (i.e., slightly less than 99% of their video frames are received within the PDB). Adding eMBB background traffic reduces the number of supported XR UEs from 4 to 3 per cell due to higher ICI and thus lower experienced SINR values if using one unique set of UPC settings. However, using distinct UPC settings for XR and eMBB UEs can maintain the XR capacity of 4 UEs per cell at an acceptable decline in best-effort eMBB throughput of a factor of 1.85.
- For the InH scenario, fractional and full path-loss compensations yield negligible differences in transmit power, PRB utilization, SINR, and consequently, XR capacity and eMBB throughput. Our findings suggest that the XR UPC setting $\{P_0^{\text{XR}} = -85, \alpha^{\text{XR}} = 0.8\}$ coupled with one of the eMBB UPC combinations in Table 3 is preferable, offering the best performance for XR and eMBB UEs. At the maximum number of supported XR UEs per cell, while still meeting the XR UEs' QoS targets of 30 ms PDB and 10 Mbps, the PRB utilization approaches 90%. As a result, the eMBB traffic does not cause an increase in interference since XR UEs utilize nearly all PRBs. This is due to the scheduler prioritizing XR traffic over eMBB traffic. This prioritization leads to extremely low eMBB cell performance, with only a few Mbps cell throughput shared among all eMBB UEs. The decrease in average eMBB cell throughput is almost equal to the increase in added XR throughput, making accurate UPC settings less critical.

The findings of this study can help cellular operators set up UPC parameters in their networks to accommodate the growing demand for XR applications in addition to currently available services. By carefully selecting UPC settings for different deployments, a balance between supporting XR experiences with strict QoS requirements and maintaining acceptable eMBB best-effort performance can be achieved.

REFERENCES

[1] *Study XR (Extended Reality) Evaluations for NR (Release 17)*, 3GPP document 38.838, Version 17.0.0, Dec. 2021.
[2] M. Gapeyenko, V. Petrov, S. Paris, A. Marcano, and K. I. Pedersen, "Standardization of extended reality (XR) over 5G and 5G-advanced 3GPP new radio," *IEEE Netw.*, vol. 37, no. 4, pp. 22–28, Jul. 2023.
[3] *Study on XR Enhancements for NR (Release 18)*, document 3GPP 38.835, Version 18.0.1, Apr. 2023.
[4] *New WID: XR (Extended Reality) for NR Phase 3*, document RP-234057, 3GPP Work Item Description, Dec. 2023.
[5] S. Dou, S. Liao, J. Wu, K. Wu, E. Chen, W. Chen, H. Shen, and N. Li, "XR quality index: Evaluating RAN transmission quality for XR services over 5G and beyond," in *Proc. IEEE 32nd Annu. Int. Symp. Pers., Indoor Mobile Radio Commun. (PIMRC)*, Sep. 2021, pp. 1–6.
[6] J. K. Sundararajan, H.-J. Kwon, O. Awoniyi-Oteri, Y. Kim, C.-P. Li, J. Damnjanovic, S. Zhou, R. Ma, Y. Tokgoz, P. Hande, T. Luo, K. Mukkavilli, and T. Ji, "Performance evaluation of extended reality applications in 5G NR system," in *Proc. IEEE 32nd Annu. Int. Symp. Pers., Indoor Mobile Radio Commun. (PIMRC)*, Sep. 2021, pp. 1–7.
[7] P. Paymard, A. Amiri, T. E. Kolding, and K. I. Pedersen, "Enhanced CQI to boost the performance of 5G-advanced XR with code block group transmissions," *IEEE Trans. Veh. Technol.*, vol. 73, no. 4, pp. 4774–4786, Apr. 2024.
[8] P. Paymard, A. Amiri, T. E. Kolding, and K. I. Pedersen, "Enhanced link adaptation for extended reality code block group based HARQ transmissions," in *Proc. IEEE Globecom Workshops (GC Wkshps)*, Dec. 2022, pp. 711–716.

[9] E. Chen, S. Dou, S. Wang, Y. Cao, and S. Liao, "Frame-level integrated transmission for extended reality over 5G and beyond," in *Proc. IEEE Global Commun. Conf. (GLOBECOM)*, Dec. 2021, pp. 1–6.

[10] P. Paymard, S. Paris, A. Amiri, T. E. Kolding, F. S. Moya, and K. I. Pedersen, "PDU-set scheduling algorithm for XR traffic in multi-service 5G-advanced networks," 2023, *arXiv:2311.08969*.

[11] B. Bojovic, S. Lagén, K. Koutlia, X. Zhang, P. Wang, and L. Yu, "Enhancing 5G QoS management for XR traffic through XR loopback mechanism," *IEEE J. Sel. Areas Commun.*, vol. 41, no. 6, pp. 1772–1786, Jun. 2023.

[12] Y. Kim, H.-J. Kwon, O. Awoniyi-Oteri, P. Hande, J. K. Sundararajan, Y. Tokgoz, T. Luo, K. Mukkavilli, and T. Ji, "UE power saving techniques for extended reality (XR) services in 5G NR systems," in *Proc. IEEE 32nd Annu. Int. Symp. Pers., Indoor Mobile Radio Commun. (PIMRC)*, Sep. 2021, pp. 1–7.

[13] D. Li, H. You, W. Jiang, X. Chen, C. Zeng, and X. Sun, "Enhanced power saving schemes for extended reality," in *Proc. IEEE 32nd Annu. Int. Symp. Pers., Indoor Mobile Radio Commun. (PIMRC)*, Sep. 2021, pp. 1–6.

[14] S. Paris, K. Pedersen, and Q. Zhao, "Adaptive discontinuous reception in 5G advanced for extended reality applications," in *Proc. IEEE 95th Veh. Technol. Conf. (VTC-Spring)*, Jun. 2022, pp. 1–6.

[15] H. Myung, J. Lim, and D. Goodman, "Single carrier FDMA for uplink wireless transmission," *IEEE Veh. Technol. Mag.*, vol. 1, no. 3, pp. 30–38, Sep. 2006.

[16] C. Ubeda Castellanos, D. L. Villa, C. Rosa, K. I. Pedersen, F. D. Calabrese, P.-H. Michaelsen, and J. Michel, "Performance of uplink fractional power control in UTRAN LTE," in *Proc. IEEE Veh. Technol. Conf. (VTC Spring)*, May 2008, pp. 2517–2521.

[17] J. Li, "Uplink power control for heterogeneous networks," in *Proc. IEEE Wireless Commun. Netw. Conf. (WCNC)*, Apr. 2013, pp. 773–777.

[18] J. E. V. Bautista, M. Malmirchegini, R. Yenamandra, and K. R. Chaudhuri, "UE-based adaptive uplink power control to enhance cell capacity of LTE systems," in *Proc. IEEE 81st Veh. Technol. Conf. (VTC Spring)*, May 2015, pp. 1–6.

[19] H. Zhang and J. Zuo, "Optimization of uplink power control parameters in wireless cellular networks," in *Proc. 5th Int. Conf. Comput. Commun. Syst. (ICCCS)*, May 2020, pp. 738–741.

[20] S. Essassi, M. Siala, and S. Cherif, "Dynamic fractional power control for LTE uplink," in *Proc. IEEE 22nd Int. Symp. Pers., Indoor Mobile Radio Commun.*, Sep. 2011, pp. 1606–1610.

[21] P. Baracca, L. G. Giordano, A. Garcia-Rodriguez, G. Geraci, and D. López-Pérez, "Downlink performance of uplink fractional power control in 5G massive MIMO systems," in *Proc. IEEE Globecom Workshops (GC Wkshps)*, Dec. 2018, pp. 1–6.

[22] M. Boussif, C. Rosa, J. Wigard, and R. Müllner, "Load adaptive power control in LTE uplink," in *Proc. Eur. Wireless Conf. (EW)*, Apr. 2010, pp. 288–293.

[23] R. Abreu, T. Jacobsen, G. Berardinelli, K. Pedersen, I. Z. Kovács, and P. Mogensen, "Power control optimization for uplink grant-free URLLC," in *Proc. IEEE Wireless Commun. Netw. Conf. (WCNC)*, Apr. 2018, pp. 1–6.

[24] R. Abreu, T. Jacobsen, K. Pedersen, G. Berardinelli, and P. Mogensen, "System level analysis of eMBB and grant-free URLLC multiplexing in uplink," in *Proc. IEEE 89th Veh. Technol. Conf. (VTC-Spring)*, Apr. 2019, pp. 1–5.

[25] W. Yang, C.-P. Li, A. Fakoorian, K. Hosseini, and W. Chen, "Dynamic URLLC and eMBB multiplexing design in 5G new radio," in *Proc. IEEE 17th Annu. Consum. Commun. Netw. Conf. (CCNC)*, Jan. 2020, pp. 1–5.

[26] K. Safjan, S. Strzyz, K. I. Pedersen, J. Steiner, and C. Rosa, "Open loop power control parameter settings impact on LTE HetNet uplink performance," in *Proc. IEEE Int. Conf. Commun. Workshops (ICC)*, Jun. 2013, pp. 1134–1138.

[27] J. Liu, D. Wang, J. Wang, J. Li, J. Pang, G. Shen, Q. Jiang, H. Sun, and Y. Meng, "Uplink power control and interference coordination for heterogeneous network," in *Proc. IEEE 23rd Int. Symp. Pers., Indoor Mobile Radio Commun. (PIMRC)*, Sep. 2012, pp. 519–523.

[28] W. Kim, Z. Kaleem, and K. Chang, "UE-specific interference-aware open-loop power control in 3GPP LTE-A uplink HetNet," in *Proc. 7th Int. Conf. Ubiquitous Future Netw.*, Jul. 2015, pp. 682–684.

[29] Y. Wang and S. Venkatraman, "Uplink power control in LTE heterogeneous networks," in *Proc. IEEE Globecom Workshops*, Dec. 2012, pp. 592–597.

[30] F. H. C. Neto, D. C. Araújo, M. P. Mota, T. F. Maciel, and A. L. F. de Almeida, "Uplink power control framework based on reinforcement learning for 5G networks," *IEEE Trans. Veh. Technol.*, vol. 70, no. 6, pp. 5734–5748, Jun. 2021.

[31] *Study on Channel Model for Frequencies From 0.5 To 100 GHz*, document 3GPP 38.901, Version 17.0.0, Mar. 2022.

[32] P. Paymard, A. Amiri, T. E. Kolding, and K. I. Pedersen, "Performance of joint XR and best-effort eMBB traffic in 5G-advanced networks," in *Proc. IEEE 97th Veh. Technol. Conf. (VTC-Spring)*, Jun. 2023, pp. 1–5.

[33] P. Paymard, A. Amiri, T. E. Kolding, and K. I. Pedersen, "Optimizing mixed capacity of extended reality and mobile broadband services in 5G-advanced networks," *IEEE Access*, vol. 11, pp. 113324–113338, 2023.

[34] F. D. Calabrese, C. Rosa, M. Anas, P. H. Michaelsen, K. I. Pedersen, and P. E. Mogensen, "Adaptive transmission bandwidth based packet scheduling for LTE uplink," in *Proc. IEEE 68th Veh. Technol. Conf.*, Sep. 2008, pp. 1–5.

[35] K. Pedersen, R. Maldonado, G. Pocovi, E. Juan, M. Lauridsen, I. Z. Kovács, M. Brix, and J. Wigard, "A tutorial on radio system-level simulations with emphasis on 3GPP 5G-advanced and beyond," *IEEE Commun. Surveys Tuts.*, early access, Mar. 27, 2024, doi: 10.1109/COMST.2024.3381669.

[36] N. Varshney, J. Zhang, J. Wang, A. Bodi, and N. Golmie, "Link-level abstraction of IEEE 802.11ay based on quasi-deterministic channel model from measurements," in *Proc. IEEE 92nd Veh. Technol. Conf. (VTC-Fall)*, Nov. 2020, pp. 1–7.

[37] M. Lampinen, F. Del Carpio, T. Kuosmanen, T. Koivisto, and M. Enescu, "System-level modeling and evaluation of interference suppression receivers in LTE system," in *Proc. IEEE 75th Veh. Technol. Conf. (VTC Spring)*, May 2012, pp. 1–5.

POURIA PAYMARD (Member, IEEE) received the B.Sc. degree in electrical engineering from Shiraz University, Shiraz, Iran, in 2016, and the M.Sc. degree in communication systems from Tarbiat Modares University, Tehran, Iran, in 2019. He is currently pursuing the Ph.D. degree with the Department of Electronic Systems, Aalborg University, in collaboration with Nokia Standards, Aalborg, Denmark. His research interests include network optimization, Extended reality communications, time-sensitive communications, and 5G/6G radio resource management.

C. SANTIAGO MOREJÓN GARCÍA received the B.Eng. degree in electronics and telecommunications engineering from Escuela Politécnica Nacional, Ecuador, in 2012, the M.Sc. degree in mobile communications from EURECOM/Télécom ParisTech, France, in 2017, and the Ph.D. degree from Aalborg University, Denmark, in 2022. Since 2012, he has worked in different private companies and public institutions, including the Ecuadorian Telecommunications Regulator (ARCOTEL), the Ecuadorian public national mobile operator (CNT), and the Swiss mobile operator SALT. He is currently with Nokia Standards as a Senior Research Specialist. His research interests include extended reality communications, radio resource management, and sidelink communications.

ABOLFAZL AMIRI received the M.S. degree in electrical and communication systems engineering from the University of Tehran, Tehran, Iran, in 2016, and the Ph.D. degree from the Department of Electronic Systems, The Technical Faculty of IT and Design, Aalborg University, Denmark, in 2022. From 2016 to 2017, he was with Huawei as an RF Engineer and a Cellular Network Optimizer. He was a Research Assistant on multi-antenna signal processing with Aalborg University, from 2017 to 2018. He is currently a Senior Standardization Research Specialist with Nokia Standards. His research interests include applications of signal processing and machine learning in wireless communications, radio resource management, and multi-antenna systems.

CLAUDIO ROSA received the M.Sc. degree in electrical engineering from Aalborg University, in 2000, the M.Sc. degree in electrical engineering (telecommunication engineering) from Politecnico di Milano, Italy, in 2003, and the Ph.D. degree from Aalborg University, in 2005. Since he joined Nokia Standards in 2005, he has contributed to the standardization of 4G and 5G systems working on uplink power control and radio resource management, carrier aggregation, dual connectivity, and unlicensed spectrum operation. He has filed more than 200 patent applications, holds more than 50 granted patents, and has co-authored more than 50 scientific publications. His current research interests include user plane protocol design for 6G, flexible duplexing, and radio enablers for extended reality applications.

BOYAN YANAKIEV received the B.Sc. degree from Sofia University, in 2006, and the M.Sc. and Ph.D. degrees from Aalborg University, in 2008 and 2011, respectively. He is currently a Senior Standardization Specialist at Nokia Standards. He is focusing on 5G-advanced and 6G topics for XR optimizations in RAN.

TROELS E. KOLDING received the M.Sc. and Ph.D. degrees from Aalborg University, Denmark, in 1996 and 2000, respectively. His M.Sc. study was achieved in collaboration with the Wireless Information Network Laboratory (WINLAB), New Brunswick, NJ, USA. Since joining Nokia Standards, in 2001, he has been active in research and management for standardization, network architecture, and portfolio management. He is currently a Distinguished Member of the Technical Staff. He is the author of more than 100 scientific publications. He holds more than 50 granted U.S. patents. His current research interests include 6G radio and network architecture, XR and GenAI-related communications, time-synchronization, and radio resource management.

KLAUS I. PEDERSEN (Senior Member, IEEE) received the M.Sc. and Ph.D. degrees in electrical engineering from Aalborg University, Aalborg, Denmark, in 1996 and 2000, respectively. He is currently a Bell Labs Fellow with Nokia Standards, leading the Radio Access Research Team, Aalborg, and a part-time External Professor with Aalborg University. He has authored publications on a wide range of topics, as well as an inventor on several patents. His current research interests include access protocols and radio resource management enhancements for 5G new radio and its evolution to 5G-advanced.